AAS 16-285

# THE LUNAR ICECUBE MISSION DESIGN: CONSTRUCTION OF FEASIBLE TRANSFER TRAJECTORIES WITH A CONSTRAINED DEPARTURE

**David C. Folta[*], Natasha Bosanac[†], Andrew Cox[‡], and Kathleen C. Howell[§]**

Lunar IceCube, a 6U CubeSat, will prospect for water and other volatiles from a low-periapsis, highly inclined elliptical lunar orbit. Injected from Exploration Mission-1, a lunar gravity assisted multi-body transfer trajectory will capture into a lunar science orbit. The constrained departure asymptote and value of trans-lunar energy limit transfer trajectory types that re-encounter the Moon with the necessary energy and flight duration. Purdue University and Goddard Space Flight Center's Adaptive Trajectory Design tool and dynamical system research is applied to uncover cislunar spatial regions permitting viable transfer arcs. Numerically integrated transfer designs applying low-thrust and a design framework are described.

## INTRODUCTION

With the increasing miniaturization of spacecraft technologies and availability of rides for secondary payloads onboard larger spacecraft supporting various missions, small spacecraft such as CubeSats offer a significantly reduced cost and development time over conventional, larger spacecraft. These benefits enable public and private entities, as well as educational institutions, to actively participate in space exploration. In fact, twelve CubeSats are intended to be launched onboard the second stage of the upcoming Exploration Mission-1 vehicle (EM-1)[1]. Following deployment, each secondary payload is injected into a translunar trajectory and must navigate to various destinations by leveraging the natural dynamics and any onboard propulsion. These missions will achieve various scientific and technology demonstration objectives, such as testing solar sail technology, investigating near-Earth asteroids, surveying the Moon for water ice, and measuring the effects of deep-space radiation on living organisms[2].

Missions involving spacecraft that are contingent upon an independent launch to attain a desired transfer trajectory or science orbit, such as the EM-1 CubeSats, face several trajectory design challenges. For these spacecraft, a fixed departure asymptote and translunar energy value limit the design space for transfer trajectories and achievable science orbits. Furthermore, CubeSats typically incorporate small propulsion systems that possess limited thrusting capabilities. The inherent uncertainty associated with both the launch date and the deployment state for secondary payloads, as well as low propulsive levels, can affect both the scope and capability of a CubeSat mission, and pose significant challenges for trajectory design.

[*] Senior Fellow, NASA Goddard Space Flight Center, Greenbelt, MD, 20771, USA
[†] Ph.D. Candidate, School of Aeronautics and Astronautics, Purdue University, Armstrong Hall, 701 W. Stadium Ave., West Lafayette, IN, 47907-2045, USA
[‡] Graduate Student, School of Aeronautics and Astronautics, Purdue University, Armstrong Hall, 701 W. Stadium Ave., West Lafayette, IN, 47907-2045, USA
[§] Hsu Lo Distinguished Professor of Aeronautics and Astronautics, School of Aeronautics and Astronautics, Purdue University, 701 W. Stadium Ave., West Lafayette, IN, 47907-2045, USA. Fellow AAS. Fellow AIAA

Trajectory design challenges are not unique to CubeSats; many other spacecraft face similar constraints during extended mission phases when propellant reserves are low or following system failures that affect a vehicle's ability to maneuver. Consider, for example, the Acceleration, Reconnection, Turbulence and Electrodynamics of the Moon's Interaction with the Sun mission, which repurposed two Time History of Events and Macroscale Interactions during Substorms vehicles for an extended mission to the Earth-Moon $L_1$ and $L_2$ regions[3]. Since neither spacecraft possessed sufficient propellant to implement a direct injection, a series of gravity assists were leveraged to reach transfers identified via dynamical systems theory. In addition to identifying low-cost transfer options, dynamical systems theory affords insight into the flow near a particular solution, which provides alternative options and facilitates design flexibility to deal with uncertainties and operational errors.

To design attainable trajectories that can achieve complex scientific goals for CubeSats with limited propulsive capability, dynamical systems techniques are leveraged. In this investigation, these techniques are applied to dynamical models of varying levels of fidelity to explore the construction of a trajectory design framework for CubeSat missions. This process is applied to the upcoming Lunar IceCube mission, which must reach a lunar orbit for scientific observation of the Moon's near polar regions after a launch as a secondary payload. Despite an energetic initial deployment state, Lunar IceCube can achieve the desired final science orbit by exploiting solar gravity to modify both its energy and phasing. To supply rapid insight into the potential geometries for the long Sun-Earth phase of the trajectory, the Circular Restricted Three-Body Problem (CR3BP) is employed. In this autonomous dynamical model, approximate bounds on the motion can be established and transfer geometries can be explained via manifolds of libration point orbits. This analysis is then transitioned to higher fidelity models including the Bicircular Four-Body Problem (BC4BP) and an ephemeris model that also includes the additional contribution of a low-thrust engine. Boundary conditions such as the initial deployment state and the final lunar science orbit are incorporated into this trajectory design framework to identify regions and geometries corresponding to feasible transfer trajectories for the Lunar IceCube mission. The constructed framework for trajectory design may also be applicable to future CubeSat missions that must meet alternative mission goals, such as re-encountering the Moon with a specific energy and/or flight duration, attaining specific Sun-Earth or Earth-Moon orbits (e.g., libration point orbits, distant retrograde orbits), or achieving a heliocentric trajectory that encounters an asteroid.

## THE LUNAR ICECUBE MISSION

Lunar IceCube, a 6U CubeSat, has been selected for participation in the Next Space Technologies for Exploration Partnerships, which leverages partnerships between public and private entities to develop the deep space exploration capabilities necessary for the next steps in human spaceflight[4]. The Lunar IceCube mission is led by the Space Science Center at Morehead State University (MSU) and supported by scientists and engineers from the NASA Goddard Spaceflight Center (GSFC), Busek, and Catholic University of America (CUA). Specifically, NASA GSFC is providing the trajectory design, maneuver and navigation planning, as well as tracking support.

The primary objective for the Lunar IceCube mission is to prospect for water in solid, liquid and vapor forms, while also detecting other lunar volatiles. Accordingly, this mission is designed to address existing strategic knowledge gaps related to lunar volatile distribution, focusing on the abundance, location and transportation physics of water ice on the lunar surface at a variety of latitudes. The required scientific observations will be performed from a highly-inclined, low-periapsis, elliptical lunar orbit using the Broadband InfraRed Compact High Resolution Exploration Spectrometer (BIRCHES). The BIRCHES instrument is designed specifically for CubeSats by GSFC as a compact version of the Origins, Spectral Interpretation, Resource Identification, Security - Regolith Explorer (OSIRIS-REx) Visible and Infrared Spectrometer as well as the Ralph spectrometer that was successfully used onboard the New Horizons mission. The design of the Lunar IceCube spacecraft, illustrated in Figure 1, also includes radiation-hardened subsystems, a JPL Iris transceiver, a high power solar panel/actuator system and a robust

multiple-processor based payload processor. These systems will enable the spacecraft to perform scientific observations for approximately six months, enabling sufficient collection of systematic volatile measurements to derive volatile cycle models. Science data and telemetry will be transmitted from the lunar vicinity at a rate of 14 kps to the controlling 21-meter ground station at MSU. The MSU antenna will also be used as the primary command and tracking station during the propulsion phase of the mission and will be used for both ranging and tracking.

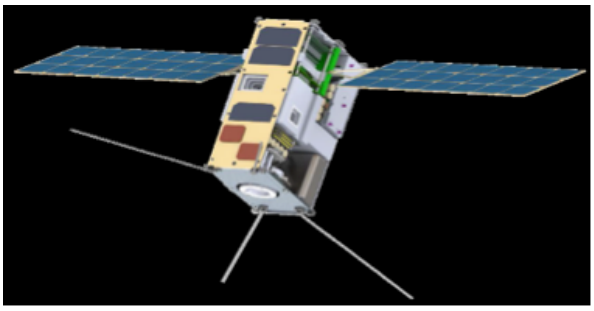

**Figure 1. Lunar IceCube preliminary spacecraft design.**

Lunar IceCube will ride onboard the EM-1 vehicle, currently scheduled for launch in late 2018. Each of the secondary payloads are deployed after Orion is injected on a lunar free-return trajectory and the Interim Cryogenic Propulsion Stage (ICPS) disposal maneuver is completed. Due to uncertainties in the ejection mechanism, Lunar IceCube's exact deployment state is not known in advance. However, with no additional maneuvers, the highly energetic nominal deployment state would result in the spacecraft quickly departing the Earth-Moon system. To decrease the spacecraft energy and achieve a transfer that approaches a low-periapsis lunar orbit, the Lunar IceCube spacecraft is equipped with a low-thrust propulsion system. This iodine-fuelled engine is a Busek Ion Thruster 3-cm (BIT-3) system, which is currently designed to deliver a maximum 1.2mN of thrust with an $I_{sp}$ of 2500s and a fuel mass of approximately 1.5 kg[5]. For the Lunar IceCube mission, the BIT-3 system enables finite duration low-thrust arcs to be introduced along the transfer trajectory.

The final lunar science orbit is constrained to meet requirements imposed by the science instruments. The BIRCHES instrument requires that observations be performed from a highly elliptical orbit to minimize thermal exposure, with an equatorial perilune altitude of 100 to 105 km. This science orbit is designed to be inertially-locked to allow measurement of lunar volatiles for the same set of representative features (by latitude, composition and age of regolith) at various times during the day. In this science orbit, the BIRCHES adjustable iris allows the instrument to act as a point spectrometer with constant footprint dimensions that are independent of the distance from the lunar surface, as the spacecraft shifts from an altitude of 100 to 250 km, i.e., from periapsis to the terminator. The spacecraft ACS system will allow the BIRCHES instrument to maintain lunar nadir-pointing during science passes.

## DYNAMICAL MODELS AND TECHNIQUES

To explore the design space for low-thrust enabled transfers that link an initial deployment state with the lunar science orbit, dynamical models of varying levels of fidelity are employed: from the CR3BP to an operational modeling environment. First, the CR3BP provides an autonomous approximation to the dynamics within the Sun-Earth system, enabling rapid and straightforward identification of the available transfer geometries over the longest segment of the Lunar IceCube trajectory. By leveraging knowledge of the dynamical structures associated with particular solutions in the Sun-Earth CR3BP, preliminary bounds can be placed on the motion. Furthermore, these types of structures that exist in the autonomous CR3BP are valuable in explaining the available transfer geometries. To incorporate the lunar influence, an additional dynamical model is employed: the BC4BP. Potential transfer geometries, identified using the CR3BP and the BC4BP, are verified using an ephemeris model that incorporates the gravity of the Sun, Earth and Moon, and an additional low-thrust force contribution via a basic model for the low-thrust BIT-3 system where thrust and $I_{sp}$ are functions of power using the standard rocket equation. As the BIT-3 system undergoes continued development, this model will be further refined. This low-thrust ephemeris model is also used to propagate motion during the initial post-deployment segment of the Lunar IceCube mission

until the first lunar encounter, as well as during the final lunar science orbit capture segment. Initial analysis in the CR3BP is performed using the Adaptive Trajectory Design (ATD) software developed by Purdue University and GSFC[6]. Designs are then transitioned to a full ephemeris model such as those found in GSFC's General Mission Analysis Tool (GMAT) and the Systems Tool Kit (STK)/Astrogator suite of tools developed by Analytical Graphics, Inc[7,8].

**Circular Restricted Three-Body Problem**

Motion within the Sun-Earth system is rapidly and reasonably approximated using the autonomous dynamics of the CR3BP. In this dynamical environment, the motion of a massless spacecraft is modeled under the influence of the point-mass gravitational attractions of two primaries: the Sun and the Earth. To enable clear visualization and identification of particular solutions, the motion of the spacecraft is described using a rotating coordinate system as depicted in Figure 2. This frame, $(\hat{x}\hat{y}\hat{z})$, rotates with the primaries as they encircle their mutual barycenter. In addition, position and velocity states locating the spacecraft are nondimensionalized. By convention, both the normalized distance between the Sun and the Earth and the mean motion of the primaries are unity. Mass quantities are nondimensionalized such that the masses of the Sun and the Earth are equal to 1-$\mu$ and $\mu$, respectively. Using these nondimensionalized quantities, the equations of motion of the spacecraft, located at $(x, y, z)$ in the rotating frame, are compactly written as[9]:

$$\ddot{x} - 2\dot{y} = \frac{\partial U}{\partial x} \qquad \ddot{y} + 2\dot{x} = \frac{\partial U}{\partial y} \qquad \ddot{z} = \frac{\partial U}{\partial z}$$

where $U$ is the pseudo-potential function, $U = \frac{1}{2}(x^2 + y^2) + \frac{1-\mu}{r} + \frac{\mu}{d}$, and $d = \sqrt{(x+\mu)^2 + y^2 + z^2}$, $r = \sqrt{(x-1+\mu)^2 + y^2 + z^2}$. When formulated in the rotating frame, this autonomous dynamical environment admits a constant energy-like integral labeled the Jacobi Constant, $C = 2U - \dot{x}^2 - \dot{y}^2 - \dot{z}^2$. At a fixed value of this integral, an infinite number of trajectories are possible within the Sun-Earth system. Any state along a time-varying solution is defined as prograde if the corresponding angular momentum vector at that instant possesses a +$z$ component, i.e., the spacecraft is traveling in a counterclockwise direction as viewed in the rotating frame of the CR3BP. Correspondingly, a state along a path that possesses a -$z$ component of the angular momentum vector is labeled retrograde. Regardless of the direction of motion, these particular solutions exhibit one of four types of behavior: equilibrium points, periodic orbits, quasi-periodic orbits and chaotic motion.

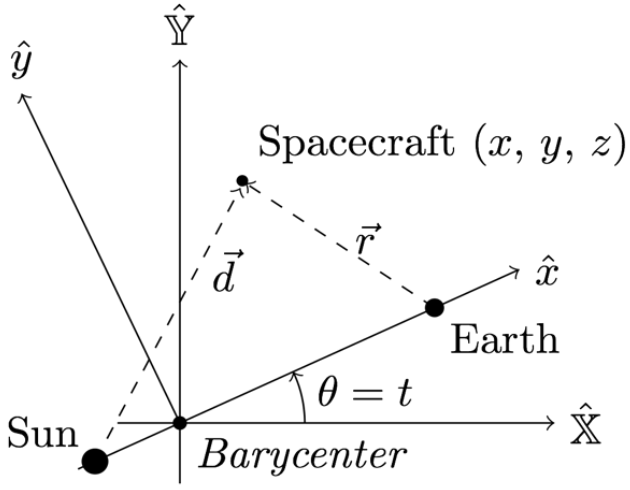


**Figure 2. System configuration for a spacecraft within the Sun-Earth CR3BP**

**Manifolds of Periodic Orbits**

Motion within the CR3BP is guided by an underlying dynamical structure that includes families of periodic orbits and their associated manifolds[10]. In the Sun-Earth system, well-known periodic orbits in the Earth vicinity include the planar Lyapunov and three-dimensional halo orbits near the $L_1$ and $L_2$ equilibrium points. Both of these families include periodic orbits that possess stable and unstable manifolds, causing nearby trajectories to naturally flow towards or away from the periodic orbit, respectively. Along these manifolds, trajectories can pass through the $L_1$ and $L_2$ gateways, departing the Earth vicinity. For planar motion, the manifold structures associated with the $L_1$ and $L_2$ Lyapunov orbits serve as separatrices, identifying the boundary between two types of motion that are qualitatively different[11]. To demonstrate this concept, consider Figure 3 which displays a sample (a) stable manifold and (b) unstable manifold associated with a Sun-Earth $L_1$ Lyapunov orbit, as generated in ATD. Using Figure 3(a) as a reference, trajectories on the blue surface lie directly on the stable manifold, which has been integrated backwards in time in a CR3BP model of the Sun-Earth system for approximately 210 days. Accordingly, these trajectories asymptotically approach the reference $L_1$ Lyapunov orbit. Motion that possesses both position and velocity states that lie within the boundaries of the blue surface pass through the $L_1$ gateway and depart the Earth vicinity. When designing CubeSat trajectories that are close to planar, the stable manifolds of the $L_1$ Lyapunov orbit can supply approximate bounds on motion, i.e., regions within the stable manifold must be avoided to ensure that a trajectory does not depart the Earth vicinity. Furthermore, this structure may influence motion near the Earth after deployment. On the contrary, motion on the green surface in Figure 3(b) lies on the unstable manifold associated with the $L_1$ Lyapunov orbit, which is integrated forward in time for 210 days. Trajectories interior to the boundaries of this manifold structure originate from the vicinity of the Sun. However, the unstable manifold may still guide motion that flows towards the Earth. In fact, arcs from both of these manifold structures may be combined to construct nearby trajectories that temporarily depart the Earth vicinity to achieve the necessary energy and phasing parameters to reach the desired lunar science orbit. Although these structures exist in the simplified and autonomous CR3BP, they are approximately retained in the true ephemeris model of the Sun, Earth and Moon, providing rapid and valuable insight into the existence and the associated boundaries for predominantly natural transfer geometries for the Lunar IceCube mission.

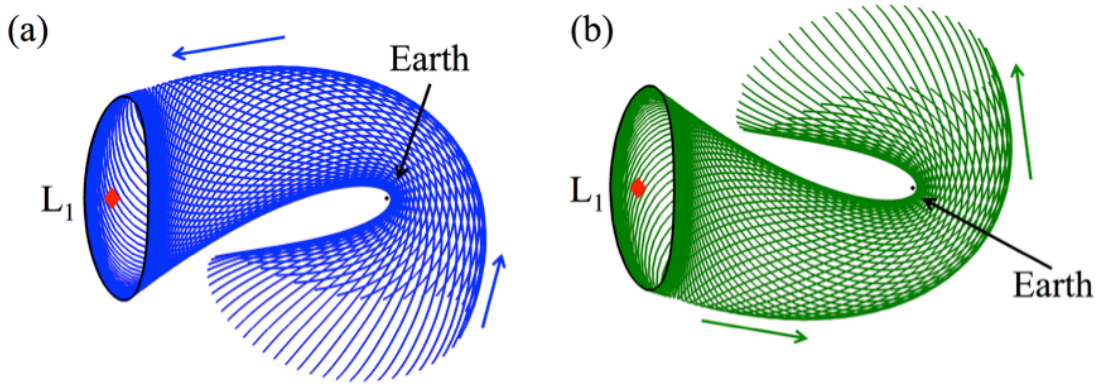


**Figure 3. (a) Stable and (b) unstable manifolds of a Sun-Earth $L_1$ Lyapunov orbit in the Sun-Earth rotating frame.**

**Mapping Techniques**

To reduce the complexity associated with visualizing a large array of trajectories or even a manifold structure that has encircled the Earth multiple times, mapping techniques are employed. To describe the spatial motion of a spacecraft at any instant of time in a nonautonomous system, six state variables are

required. Assuming solely planar motion, the dimensions reduce to four, but visualization is still not straightforward. To overcome the challenges associated with visualizing these states along a trajectory, Poincaré mapping is employed. In fact, this technique leverages a higher-dimensional surface, typically labeled a hyperplane, or a surface of section[12]. These surfaces of section can simply employ geometry and take the form of straightforwardly-visualized planes such as $y = 0$ or $z = 0$, or even functional events such as apoapsis, periapsis, or time. The intersection of a trajectory with this surface of section produces a finite sequence of points, eliminating one dimension. For a range of trajectories, these intersections produce a map that can represent the flow. Limiting the Jacobi constant value reflected in the trajectories captured by the map further reduces the free dimensions representing the state. In fact, for planar motion, a two-dimensional Poincaré map can exactly represent the complete state vector. However, for spatial motion, some information can be lost in the mapping process. As an example of the utility of mapping techniques, however, consider solely planar motion along a stable manifold associated with a Sun-Earth $L_1$ Lyapunov orbit as depicted in Figure 4(a). This orbit, displayed in black, exists at a Jacobi constant of $C = 3.000884$ and encircles the $L_1$ equilibrium point, located by a red diamond. The stable manifold surface is computed by isolating the stable mode, as constructed from the monodromy matrix, as it evolves along the periodic orbit. After seeding states along the orbit and adding a small perturbation in the direction of the stable eigenvector, integration backwards in time produces the stable manifold surface as depicted in blue. Propagation proceeds until the first apoapsis with respect to the Earth. Note that the arrows indicate the direction of motion forward in time, as the flow along the manifold surface asymptotically approaches the periodic orbit. Integrating this planar manifold surface backwards in time produces a large set of trajectories that is difficult to visualize as the manifold continues to encircle the Earth. By employing a Poincaré mapping technique, the first apoapses along the stable manifold are captured on a surface of section and yield a single curve, displayed in magenta. Additional apoapses along the manifold surface produce additional curves. These apoapses are straightforwardly represented on a Poincaré map in configuration space, as depicted in Figure 4(b). States that lie inside this curve depart the Earth vicinity through the $L_1$ gateway, while states outside of the magenta set of apoapses may potentially remain within the Earth vicinity for a given time span. Such qualitative analysis is straightforward through the application of Poincaré mapping strategies and may be valuable for approximate representation of spatial motion, even in nonautonomous dynamical models.

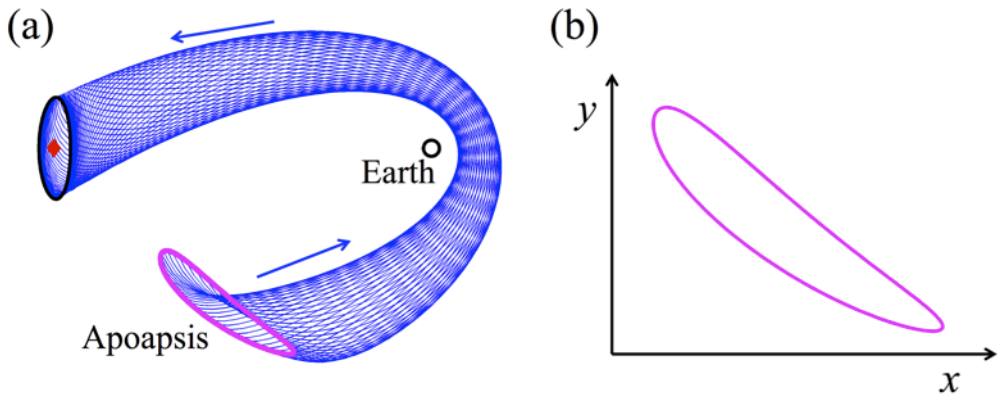


**Figure 4. Representation of (a) stable manifold tube associated with an L1 Lyapunov orbit in the Sun-Earth system via a (b) apoapsis map plotted in configuration space.**

**Bicircular Four-Body Problem**

Though the CR3BP provides reasonable approximations for many trajectories, the inclusion of the gravity of a fourth body (i.e., the Moon) can significantly impact a trajectory. To improve the fidelity of arcs computed in the CR3BP, the BC4BP is employed[13,14]. This dynamical model governs the motion of a comparatively small body, i.e., a spacecraft, under the influence of three primary gravitational bodies, the

Sun, Earth, and Moon. Given simplifying assumptions that are consistent with the CR3BP, the BC4BP models the motion of the spacecraft within the coordinate frame ($\hat{s_x}\hat{s_y}\hat{s_z}$), as depicted in Figure 5, which rotates with the Sun and $B_2$, the Earth-Moon barycenter. The motion of $B_2$ about the system barycenter, $B_1$, is assumed to be circular. Similarly, the motion of the Earth and Moon are also modeled as circular about their mutual barycenter $B_2$. Thus, the motion of the primaries is not coherent but the subsequent spacecraft trajectory can still be a good approximation to the actual path. Coordinates in this rotating frame are nondimensionalized such that the distance between the Sun and $B_2$, as well as the mean motion of the rotating frame, $\dot{\theta}$, are both equal to a constant value of unity. Furthermore, masses in the BC4BP are normalized using the total mass of all three primaries within the system. The equations of motion governing the spacecraft resemble the CR3BP equations of motion, and are compactly written as:

$$\ddot{x} - 2\dot{y} = \frac{\partial U_4}{\partial x} \qquad \ddot{y} + 2\dot{x} = \frac{\partial U_4}{\partial y} \qquad \ddot{z} = \frac{\partial U_4}{\partial z}$$

where the corresponding pseudo-potential function is equal to $U_4 = \frac{1}{2}(x^2 + y^2) + \frac{1-\mu}{s} + \frac{\mu-\nu}{e} + \frac{\nu}{m}$ and $s$, $e$, and $m$ are the magnitudes of the vectors from the Sun, Earth, and Moon to the spacecraft, respectively. Furthermore, $\mu$ and $\nu$ are the non-dimensional masses of the Earth-Moon system and the Moon, respectively. Due to the gravitational influences of the Earth and Moon, which are not stationary within the rotating frame, the BC4BP is nonautonomous and does not admit an integral of motion.

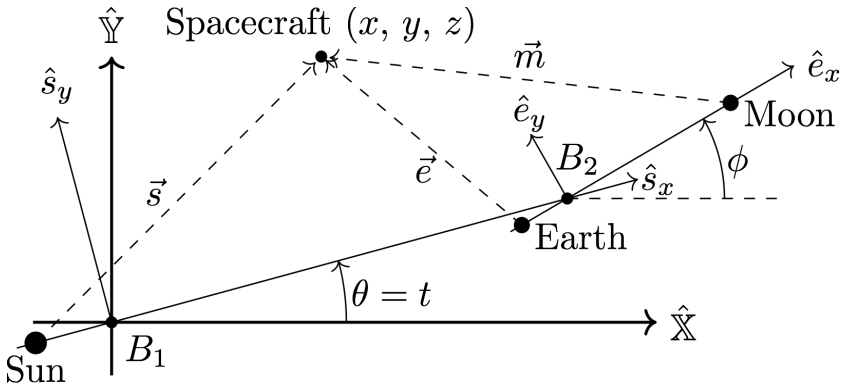


**Figure 5. System configuration for a spacecraft within the Sun Earth-Moon BC4BP.**

**Ephemeris Model**

To incorporate the true, noncircular motion of the Sun, Earth and Moon, a high-fidelity ephemeris model is employed to generate accurate end-to-end trajectories. Interactive trajectory design environments including GSFC's GMAT and AGI's STK both provide operational-level ephemeris models of the solar system as well as additional perturbations such as solar radiation pressure and higher-order gravitational contributions. Furthermore, these software packages can also incorporate propulsive capability in the form of a low-thrust engine. Trajectories that are rapidly and straightforwardly generated using the simplified models in the CR3BP and BC4BP may be approximately reproduced using GMAT or STK and then corrected to recover a continuous end-to-end transfer.

## SAMPLE MISSION TRANSFER TRAJECTORIES

Following ejection from the ICPS, Lunar IceCube is designed to apply a low-thrust maneuver using the BIT-3 propulsion system over several days to modify the outgoing trajectory. Without any control, the spacecraft quickly escapes the system. However, application of a finite duration burn alters the lunar B-plane and energy. This modification to the lunar flyby conditions produces a trajectory that temporarily follows a Sun-Earth transfer arc prior to returning to the lunar vicinity. In combination with low-thrust maneuvers within the Sun-Earth system, these transfers allow the solar and lunar perturbations to raise the

perigee to match the lunar orbit radius, adjust the timing of the lunar encounter, rotate the line of apsides, and achieve a ballistic lunar encounter that reduces lunar capture ΔV requirements, such that the lunar C3 orbital energy is below -0.05 $km^2/s^2$. Furthermore, this transfer and capture design minimizes the number of passages through the radiation belts.

To validate the overall design process for trajectories that meet the spacecraft constraints of mass, area, propulsion capability and thrust levels, several point designs have been numerically generated using a basic understanding of the Sun-Earth dynamical system structure and targeting the outgoing lunar flyby. These designs, depicted in Figure 6, are simulated via operational tools and resemble Sun-Earth manifold structures, while also yielding capture into a lunar science orbit. They depict the variation in the possible transfer trajectories given a fixed outgoing asymptote, altered via low-thrust accelerations. In these designs, the goal is articulated to achieve a return to the lunar orbit region while minimizing multiple perigee passes to reduce or eliminate radiation effects on the instrument. Each of these designs use the same initial EM-1 launch epoch of December 15, 2017 and the same post ICPS deployment state made available at the time of the Lunar IceCube proposal. The post ICPS deployment information will be updated once the EM-1 design has been finalized, thus requiring a redesign of the trajectory and a complete understanding of the transfer trajectory trade space.

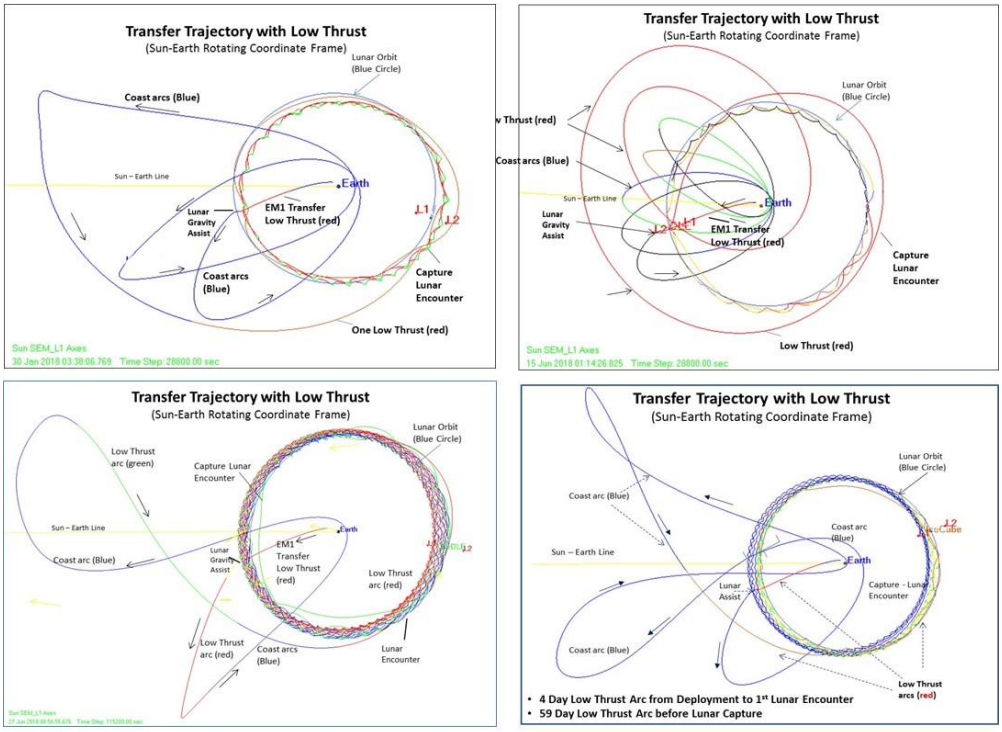


**Figure 6. Sample transfer trajectories determined using operational-level software for the same initial deployment state and epoch, plotted in the Sun-Earth rotating frame.**

## TRAJECTORY DESIGN FRAMEWORK

Although feasible end-to-end transfers may be obtained within an operational modeling environment, a dynamical systems approach offers significant insight into the available transfer geometries and the corresponding regions of existence. Individual point solutions may be highly sensitive to uncertainties in both the deployment state and epoch, as well as any additional on-orbit perturbations. In fact, for relatively large perturbations, a spacecraft may not possess sufficient propulsive capability to achieve a given

reference trajectory. Alternatively, another transfer geometry may provide an operationally-feasible solution. To facilitate the identification and computation of these solutions, a trajectory design framework is constructed and demonstrated. First, the complete transfer trajectory is split into three segments: the post-deployment lunar encounter, the Sun-Earth-Moon transfer, and the lunar approach. Concepts from dynamical systems theory are applied to models of varying levels of fidelity, from the CR3BP to ephemeris, over each segment. Next, mapping techniques are employed to identify connections between available trajectory arcs. Using the resulting analysis, a reasonable initial guess is obtained for corrections in an ephemeris model to obtain a high-fidelity, low-thrust enabled, end-to-end transfer.

**Post-Deployment Lunar Encounter**

Following deployment of the Lunar IceCube spacecraft, the low-thrust BIT-3 engine is leveraged to target the desired lunar flyby conditions. In the absence of a low-thrust burn, the Lunar IceCube spacecraft would quickly escape the Earth-Moon system. When activating the BIT-3 low-thrust system over the speculated 4.5 day arc between deployment and the lunar flyby, the spacecraft is guided along a path that remains within the Earth vicinity and eventually returns to the Moon. The thrust direction clearly impacts the lunar flyby conditions: while it is most effective to thrust in the anti-velocity direction to reduce the spacecraft energy at flyby, small deviations from this thrust direction may significantly impact the lunar flyby conditions. Beyond the lunar flyby, low-thrust may be employed to shift the first apogee in configuration space and potentially enable links to other transfer geometries. To demonstrate the effect of the low-thrust force on the first apogee, GSFC's GMAT software is used to propagate the motion of the spacecraft following a fixed post-deployment lunar flyby. Several simulations are performed for this fixed flyby state by varying (i) the time to coast naturally post-perilune, and (ii) the subsequent burn time. Furthermore, the thrust is applied either along the velocity or anti-velocity vector to demonstrate the effect of the thrust direction. The resulting planar projections of the positions of the first apogees for various coast and burn times, thrusting either along or against the velocity direction, are displayed in Figure 7 in the Sun-Earth rotating frame. In Figure 7(a), these planar projections of the apogees are colored by Jacobi constant, while in Figure 7(b) the apogees are colored by the epoch as expressed in modified Julian date. These guided apogees approach the naturally-propagated apogee, indicated by a diamond marker, as the thrust time reduces to zero. Apogees that occur closer to Earth, within the *xy* plane of the Sun-Earth rotating frame, correspond to thrust that is applied in the anti-velocity direction to slow the spacecraft. Conversely, thrust applied along the velocity vector results in apogees that lie further from the Earth in the *xy* plane of the Sun-Earth rotating frame. Mapping strategies are useful in visualizing the effect of thrusting after the post-deployment lunar encounter on the set of attainable apogees, thereby facilitating the search for links to the longer Sun-Earth-Moon segment of the Lunar IceCube transfer.

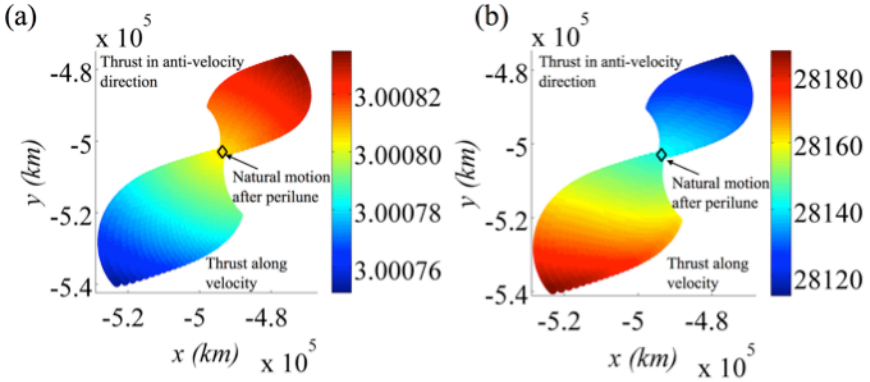


**Figure 7. Planar projection of achievable first Earth apoapses plotted in the Sun-Earth rotating frame for a fixed lunar B-plane target and epoch, colored by (a) Jacobi constant and (b) epoch in terms of modified Julian date.**

**Sun-Earth-Moon Transfer**

Following the post-deployment encounter with the Moon, the Lunar IceCube transfer trajectory leverages the gravity of the Sun prior to capturing into the lunar science orbit. While this longest trajectory segment remains within the Earth vicinity, it leverages the natural dynamical structures within the Sun-Earth system to modify both its energy and phasing. To reduce the number of deterministic thrusting arcs required along this portion of the Lunar IceCube mission trajectory, predominantly natural motions are sought. Accordingly, mapping techniques are employed to explore the geometry and the natural flow that persist within the Earth vicinity. These maps are first constructed in the CR3BP, and then the BC4BP, to explain the geometry of the transfers that are constructed in these simplified dynamical models.

*SE Transfer Apoapsis Maps in the CR3BP*

To simplify the visualization of a large array of trajectories at a single energy level in the CR3BP, apoapsis maps are employed. Construction of these maps is straightforward and a sample value of the Jacobi constant, set equal to C = 3.0088, demonstrates their use. At this value of the Jacobi constant, both the $L_1$ and $L_2$ gateways are slightly open and only a small number of trajectories depart the Earth vicinity, enabling a clear demonstration of the analysis employed in this investigation. Feasible initial conditions in the Earth vicinity are seeded between the $L_1$ and $L_2$ gateways, and take the form of an apoapsis with respect to the Earth. For a state to be considered an Earth apoapsis, it must possess a relative position vector $r = [x - 1 + \mu, y, z]$ that is instantaneously perpendicular to the velocity vector, $v = [\dot{x}, \dot{y}, \dot{z}]$. Furthermore, the radial acceleration of an apoapsis must be negative. For this investigation, only planar motion is considered when creating apoapsis maps in the CR3BP and the BC4BP. Although trajectories within the true ephemeris model exist in three-dimensional space, the spatial component of motion along each sample transfer is small. Accordingly, planar motion in the CR3BP offers a valuable preliminary approximation. The direction of velocity at each apoapsis is selected uniformly across the entire map to produce states that are either prograde with respect to the Earth or retrograde, i.e., counter-clockwise or clockwise, respectively. Thus, for various combinations of the planar position components, the direction of the velocity is determined via orthogonality. For a specified value of the Jacobi constant, the unit vector along the velocity direction is scaled using the velocity magnitude, computed as $v = \sqrt{2U - C}$. Each initial apoapsis, seeded within the vicinity of the Earth, is then propagated forward for a specified number of revolutions about the Earth from the perspective of the rotating frame. Initial conditions that produce trajectories that either impact the Earth or pass through the $L_1$ or $L_2$ gateways are discarded. The remaining initial conditions are plotted in configuration space, producing a composite representation of the initial apoapses of trajectories that remain within the Earth vicinity, as predicted by the Sun-Earth CR3BP. As an example, two apoapsis maps are displayed in Figure 8 for the Jacobi constant value $C$ = 3.00088, representing trajectories that complete one revolution about the Earth without departing through the $L_1$ or $L_2$ gateways or impacting the Earth. In Figure 8(a), each initial apoapsis is prograde, while Figure 8(b) displays only retrograde apoapses. For convenience, these maps are depicted using Earth-centered rotating coordinates. Grey shaded portions in each figure indicate forbidden regions, where motion cannot extend within the phase space of the CR3BP for the specified value of the Jacobi constant. Blue points locate apoapses that produce trajectories that remain within the Earth vicinity for one revolution and do not impact the Earth. White regions, however, result in trajectories that do not fulfill these criteria. Furthermore, red diamonds locate the equilibrium points, while a small light blue circle indicates the location of the Earth and the green circle represents a circular approximation to the orbit of the Moon. These apoapsis maps supply an approximate, yet rapid, representation of natural motions that may be incorporated into the CubeSat transfer strategy.

When supported by concepts from dynamical systems theory, apoapsis maps supply insight into some preliminary bounds on the feasible regions of motion near the Earth. For instance, consider the prograde apoapsis map in Figure 8(a). The white region in the lower left quadrant is contained within the curve

corresponding to the first apoapses along the $L_1$ Lyapunov stable manifold, similar to the curve depicted in Figure 4. Specifically, each apoapsis within this white region quickly departs the Earth vicinity through the $L_1$ gateway. Similarly, the white region in the top right quadrant of Figure 8(a) is enclosed by the first apoapses along $L_2$ Lyapunov stable manifold at this value of Jacobi constant. For motion in the CR3BP to remain within the Earth vicinity, these two white regions should be avoided, creating approximate bounds on the motion during this segment of the transfer. Using Figure 8(b) as a reference, the set of retrograde apoapses that produce feasible trajectories are separated by a thick white band. In fact, apoapses within this white region produce trajectories that resemble conics that quickly impact the Earth. As the model fidelity is improved, these preliminary bounds may shift and change size within the phase space. However, knowledge of these regions corresponding to known dynamical structures may supply preliminary insight into the sensitivity of any nearby trajectories and facilitate explanation of the available transfer geometries.

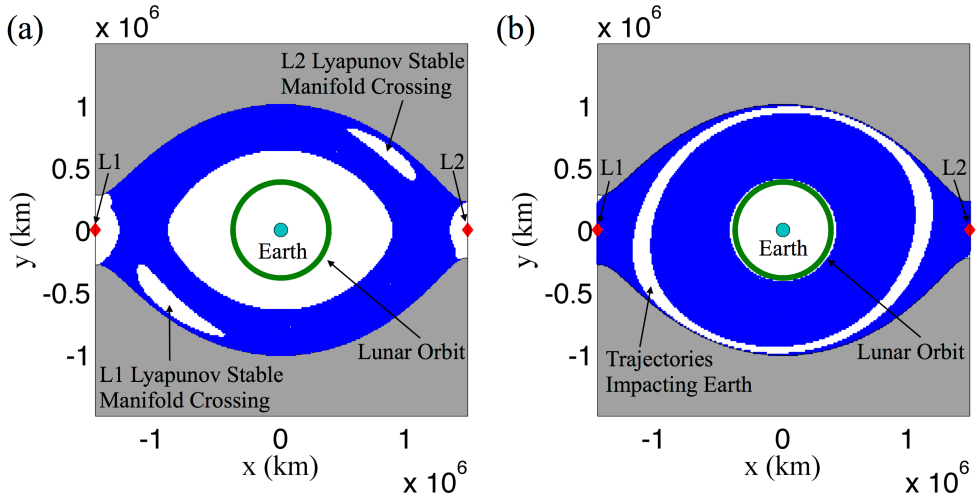


**Figure 8. Apoapsis maps in the CR3BP at $C = 3.00088$ for (a) prograde and (b) retrograde initial conditions. Blue regions indicate initial apoapses of feasible trajectories that remain within the Earth vicinity for one revolution.**

*Feasible Transfer Regions*

Regions in the Earth apoapsis maps in Figure 8 corresponding to transfers that remain in the Earth vicinity can be differentiated by their geometries to guide numerically targeting outgoing lunar flyby conditions which subsequently place the Lunar IceCube spacecraft on a natural transfer that requires little propulsive effort. To demonstrate the identification of feasible transfer regions and their associated geometries, consider an apoapsis map constructed using prograde initial conditions at $C = 3.00088$ for trajectories that complete two revolutions around the Earth, as depicted in Figure 9. Recall that gray shaded portions of the figure indicate forbidden regions, while red diamonds locate the equilibrium points, the light blue circle at the center indicates the location of the Earth and the purple curve depicts the lunar orbit, approximated as circular. On this apoapsis map, apoapses for each feasible transfer region are colored by the geometry of the subsequent transfer path, determined using the velocity direction at each apoapsis, i.e. prograde or retrograde. Specifically, blue regions in Figure 9 indicate transfers that possess only apoapses that are prograde, such as the transfer displayed in the bottom left inset. The feasible transfer regions colored green, however, correspond to trajectories that possess one retrograde apoapsis, as displayed in the top right inset of Figure 9. Note that these green feasible transfer regions appear to hug the white regions corresponding to the apoapses along the $L_1$ and $L_2$ Lyapunov stable manifolds, indicating that these transfers leverage the nearby natural dynamical structures. Finally, red-colored feasible transfer regions represent trajectories

where the second and final apoapses are both retrograde as depicted in the bottom right inset of Figure 9. This feasible transfer region lies close to the zero velocity curves of the CR3BP and the transfers resemble the sample end-to-end trajectory in the bottom right corner of Figure 6, constructed as a point solution using an operational modeling environment.

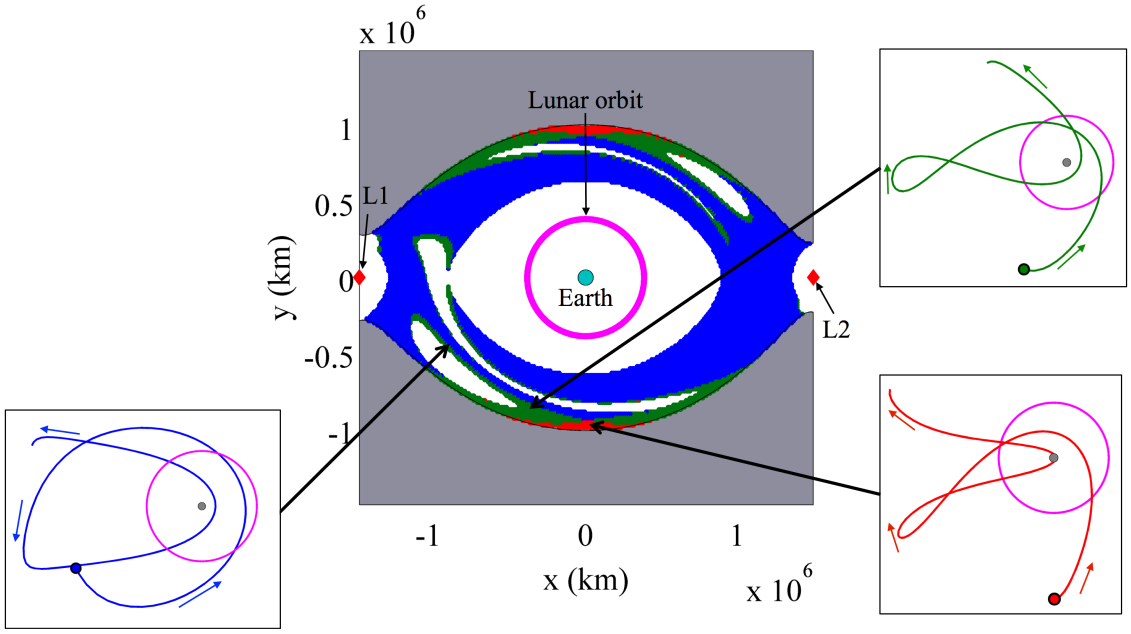


**Figure 9. Apoapsis map in the CR3BP at $C = 3.00088$ for prograde initial conditions. Blue, red and green regions indicate initial apoapses of feasible trajectories that remain within the Earth vicinity for two revolutions, with each color corresponding to a different transfer geometry illustrated via the inset images.**

*Sun-Earth-Moon Transfer Apoapsis Maps in the BC4BP*

The mapping techniques employed in the CR3BP are applied to the nonautonomous BC4BP. Recall that in the BC4BP, an epoch is identified with each state along a trajectory. Accordingly, each apoapsis map in the BC4BP is constructed for a single initial epoch; the remainder of the map construction process, however, is consistent with the CR3BP. To compare apoapsis maps created for two models of different fidelity, consider Figure 10. This map is constructed in the BC4BP for an initial lunar angle – defining the epoch - indicated by the orange diamond. The blue, green and red points in this map summarize prograde apoapses that produce feasible trajectories remaining within the Earth vicinity. The specific color scheme used in Figure 10 is consistent with the color scheme employed in Figure 9, with blue, red and green regions indicating the trajectory geometries corresponding to each feasible transfer region. Using Figure 10 as a reference, the white region in the bottom left quadrant, corresponding to apses within the stable manifold of the $L_1$ Lyapunov orbit, has shifted in configuration space due to the additional gravitational influence of the Moon. Furthermore, new white regions have appeared as additional apoapses lead to trajectories that either depart the Earth vicinity via the $L_1$ and $L_2$ gateways or crash into the Earth or Moon. However, each of the transfer geometries identified in the CR3BP using Figure 9 still exist in the BC4BP for this initial lunar angle (epoch), but are shifted in configuration space. Additionally, these mapping techniques, derived from dynamical systems analysis, facilitate the visualization of a wide array of trajectories and identification of the corresponding geometries, while also guiding the connection to other segments of the trajectory.

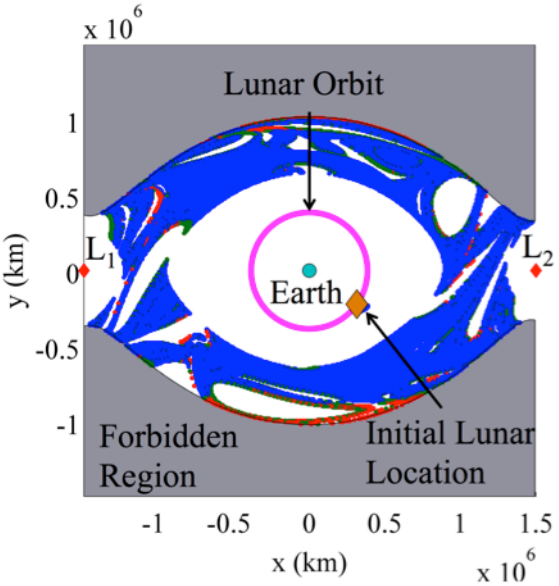


**Figure 10. Apoapsis map in the BC4BP at *C* = 3.00088 for prograde initial conditions. Blue, red and green regions indicate initial apoapses of different trajectory geometries that complete two revolutions within the Earth vicinity.**

### Lunar Approach

To enable the science instruments onboard the Lunar IceCube spacecraft to gather information about lunar water and other volatiles, constraints are imposed on the final lunar science orbit. In fact, these instruments constrain the lunar ground track, requiring the observations to occur from a highly-inclined elliptical lunar orbit with the desired orbital period. This constrained science orbit, depicted in green in Figure 11, is characterized by a perilune altitude of between 100 and 105 km, with perilune positioned over the lunar equator, and an apolune altitude of 5000 km. Furthermore, the orbit is constrained to possess an inclination within the range 65-75 degrees. The remaining orbital elements are left unconstrained, and may be employed as variables to locate an end-to-end transfer trajectory that arrives in a feasible lunar science orbit.

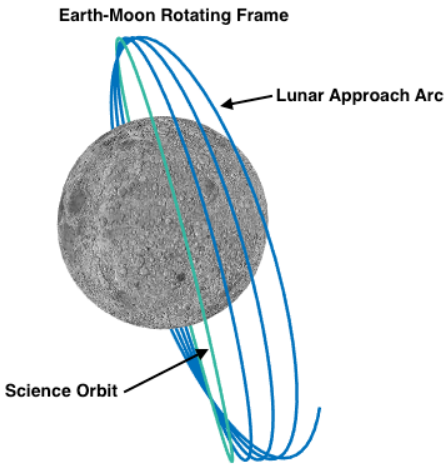


**Figure 11. A sample science orbit (green) and a connecting low-thrust enabled lunar approach arc (blue) displayed in the Earth-Moon rotating frame.**

Consistent with the two previous transfer segments, i.e., the post-deployment lunar encounter as well as the Sun-Earth-Moon transfer, a subsequent link to a feasible lunar science orbit may be both challenging and computationally expensive to locate, with limited guidance available. Insight from manifold computation techniques is again valuable. In particular, a lunar science orbit is generated that possesses an inclination, perilune altitude and apolune altitude within the acceptable ranges. The epoch and right ascension of the ascending node (RAAN) are then freely selected to orient the orbit. For a single state along the sample science orbit, identified via the true anomaly (TA), simulations in GMAT are accomplished in reverse time with the low-thrust engine

activated and directed along the anti-velocity vector. The spacecraft spirals away from the lunar science orbit in reverse time, until it pierces a geometric hyperplane defined in configuration space to be perpendicular to the Earth-Moon line and slightly displaced outside of the $L_2$ point. Selection of this hyperplane is driven by the characteristics of the desired motion. In particular, the low-thrust engine essentially increases the energy of the spacecraft. Simultaneously, the zero velocity curves recede further from the Moon, eventually opening the $L_1$ and $L_2$ gateways. To escape the vicinity of the Moon, the spacecraft can pass through the Earth-Moon $L_2$ gateway and merge into the Sun-Earth segment of the transfer trajectory. Accordingly, a hyperplane located near the Earth-Moon $L_2$ point effectively captures a path with the desired itinerary. A zoomed-in view of the planar projection of a sample lunar approach arc generated via this process is displayed in the Earth-Moon rotating frame in Figure 12(a). The black arrow indicates the direction of motion in forward time, while the asterisks locate the equilibrium points. The green vertical line represents a planar projection of the near-$L_2$ hyperplane used to locate paths that depart through the Earth-Moon $L_2$ gateway. In forward time, motion along this arc approaches this lunar science orbit and results in capture when the low-thrust burn ceases. Trajectories that cross the near-$L_2$ hyperplane are then propagated further in reverse time until apogee for a range of thrust durations, up to a maximum of 15 days. This concept is depicted near the Moon in Figure 11 via a blue arc. Computation of these lunar approach arcs is repeated for various thrust durations, TA, RAAN, and a fixed epoch. Projections of these paths onto the ecliptic plane are plotted in Figure 12(b) in the rotating frame of the Sun-Earth system for a fixed final science capture epoch of September 28, 2018 and a RAAN equal to 25 degrees for states located at a true anomaly of 0 degrees. Each arc within this figure is colored by the low-thrust burn duration after crossing the near-$L_2$ hyperplane, and the black arrow indicates direction of motion in forward time. As evident in this figure, the use of the 1.2mN BIT-3 engine can shift the first apogee of the lunar approach arc within configuration space, effectively enabling the targeting of a continuous trajectory that links the post-deployment state to the lunar science orbit.

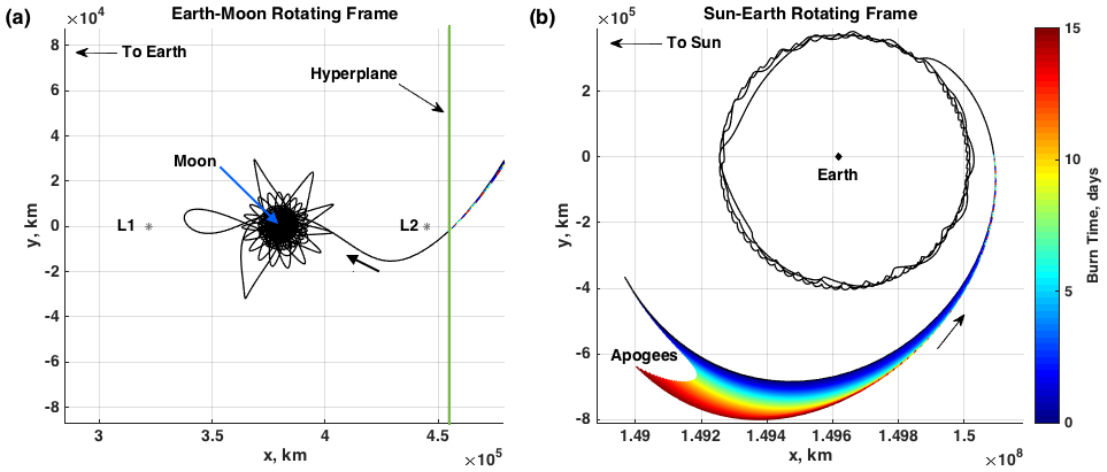


**Figure 12. (a) Lunar IceCube spacecraft approaches the Moon and decreases its orbital radius via a long-duration low-thrust maneuver. (b) Varying the burn duration on reverse-time-propagated arcs produces a range of apogees.**

To facilitate a connection with the previous Sun-Earth-Moon trajectory segment, mapping strategies are employed to visualize apogees that result in a low-thrust enabled capture into the final science orbit. Using the mapping technique to represent science approach arcs, the process is repeated for discretely sampled states along various science orbits with selected values of RAAN and TA. Figure 13 displays the planar projections of the apogees which result in lunar capture, at an epoch of September 29, 2018, into a science orbit with a value of RAAN discretely sampled within the range [0, 360] degrees and true anomalies

sampled within the range [0, 360] degrees. Although Figure 13 only displays a projection onto the ecliptic plane, each apoapsis typically possesses a small out-of-plane component. Accordingly, such a visualization may supply a preliminary approximation of the true locations of the computed apogees. These apoapses are represented in the Sun-Earth rotating frame and are colored by parameters that can guide the location of continuous transfers: in Figure 13(a), apses are colored by Jacobi constant, while the colorbar in Figure 13(b) indicates the lunar angle. Maps such as Figure 13 can guide selection of trajectories that approach a feasible lunar science orbit and the potential connection to the Sun-Earth transfer segment.

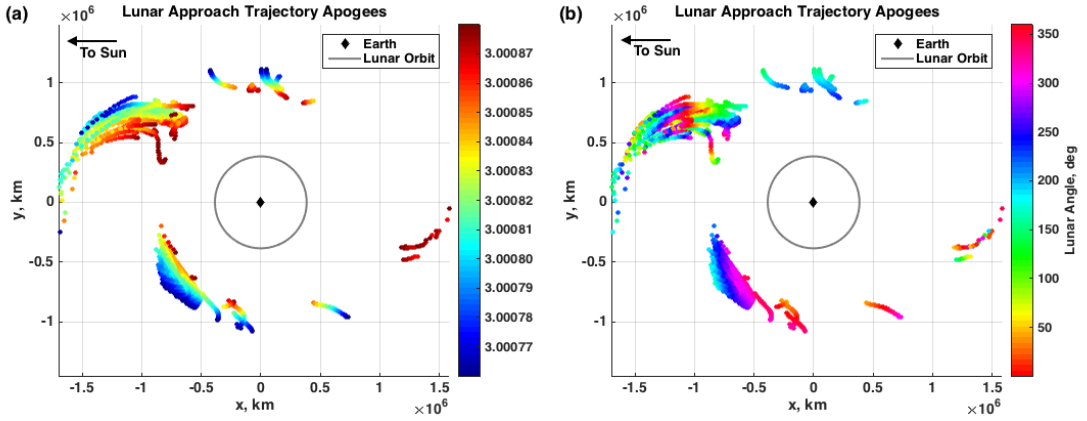


**Figure 13. Planar projections of apogees (both prograde and retrograde) on trajectories arriving at a lunar science orbit on September 29, 2018. Apses are colored by instantaneous values of (a) Jacobi Constant and (b) lunar angle.**

### End-to-End Transfer: Connections Between Transfer Segments

To validate the proposed trajectory design framework, a sample trajectory is split into the three mission segments and compared to the transfer options identified by the tools within this framework. Consider the previously developed point solution as seen in the lower right panel in Figure 6; this solution is constructed using operational-level ephemeris software. This sample trajectory is reproduced in Figure 14. The transfer begins at the current EM-1 deployment state; shortly thereafter, a 3.8 day low-thrust arc is activated until just before lunar periapsis to decrease the orbital energy and to target a lunar B-plane crossing that produces a trajectory which remains within the Earth vicinity. This multi-day maneuver is represented by a red arc segment in Figure 14. Following the first lunar flyby, the spacecraft initiates a long coast arc (blue) and passes through three apogees over 173 days before beginning a 70 day low-thrust burn, colored red, to capture around the Moon and achieve the desired science orbit. The end-to-end path requires three arcs, one for each mission segment. Once the arcs are designed, individuals are linked to deliver a continuous path.

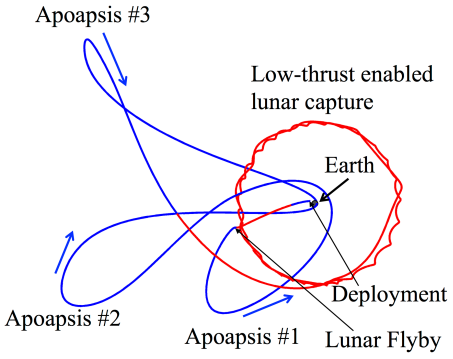


**Figure 14. Sample Lunar IceCube transfer in the Sun-Earth rotating frame produced using an ephemeris model, with blue segments indicating natural coasting arcs and red segments depicting low-thrust arcs.**

*Linking the Post-Deployment Lunar Encounter to the Sun-Earth-Moon Transfer*

To ensure that the Lunar IceCube spacecraft remains within the Earth vicinity, the post-deployment lunar encounter path must link to the feasible transfer regions within the Sun-Earth system. This connection is confirmed by comparison of the first apoapsis along the sample transfer to a map constructed in the BC4BP. Using ephemeris data, the first apoapsis along the trajectory in Figure 14 occurs at an epoch of 28118.12 in modified Julian date form, and possesses a Jacobi constant value approximately equal to 3.001225. While this Jacobi constant is above the values corresponding to $L_1$ and $L_2$ at this instant along the trajectory, recall that in a nonautonomous system, $C$ is no longer constant. At this apogee, the Moon is located at an angle of approximately 35 degrees below the line from Earth to $L_2$. Using this initial lunar angle, along with the value of $C$ = 3.001225, an apoapsis map is constructed using the BC4BP for trajectories that encircle the Earth twice. This map is displayed in Figure 15(a) and uses a color scheme consistent with the previous maps presented in this investigation. Each initial apoapsis is assumed to be planar and prograde with respect to the Earth, with feasible transfer regions colored by the geometry of the resulting transfers. An orange diamond locates the initial lunar location. A purple-filled diamond in the bottom left quadrant of the apoapsis map indicates a planar projection of the position of the first apogee along the sample transfer. This apogee occurs in a region of the map, appearing in the zoomed-in view in Figure 15(b), where there are blue, red and green points, indicating that the geometries of the nearby transfers are sensitive to state uncertainties. Due to the presence of a nearby white region, significant uncertainty in the first apogee may result in a transfer that either escapes the Earth vicinity or impacts one of the primaries. Selecting a nearby red apogee from the map locates transfers that begin with a prograde initial apogee and possess two retrograde apogees along the path, similar to the sample solution. Integrating the selected initial apogee forward in the BC4BP produces the transfer depicted in Figure 15(c), which resembles the sample transfer in Figure 14. Note that the sample transfer is three-dimensional in the true ephemeris model. Accordingly, the planar transfer in Figure 15 provides a rapid and preliminary approximation to nearby complex motions that may otherwise be challenging to identify. Furthermore, this analysis supplies initial guesses for the Sun-Earth transfer arc prior to connecting each of the three segments via corrections in an ephemeris model.

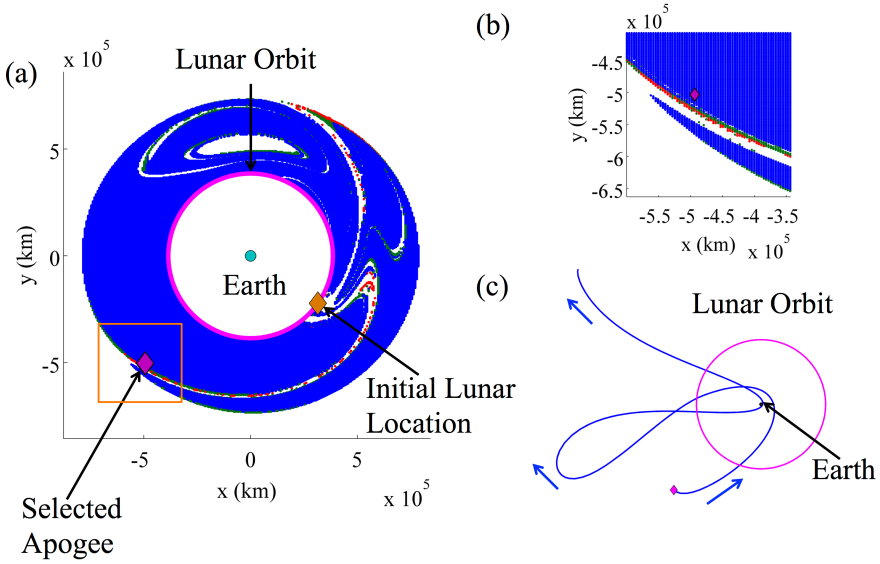


**Figure 15. (a) Comparison of the first apogee along the sample trajectory on an apoapsis map constructed in the BC4BP for $C$ = 3.001225 and initial lunar angle of 35 degrees below the Earth-$L_2$ line, (b) zoomed-in view of map region near the highlighted apogee and (c) planar trajectory propagated in the BC4BP, resembling sample transfer.**

*Linking the Sun-Earth-Moon Transfer to the Lunar Approach*

To complete the transfer, candidate connections between the Sun-Earth-Moon transfer segment and lunar approach segment are identified by locating apogees from both segments that occur in similar regions of space at similar epochs, and possess a similar energy. By locating nearby apogees, connections between arc segments are identified to facilitate construction of an end-to-end trajectory that links a feasible post-deployment flyby to capture into the final science orbit. Given two apses that are close in their planar projections on a map, a similar value of the Jacobi constant indicates that the velocities at the apses are also similar in magnitude and direction. Accordingly, minimal corrective maneuvers may be required to join the two arcs emanating from these apses. Furthermore, a good initial guess for a continuous transfer must

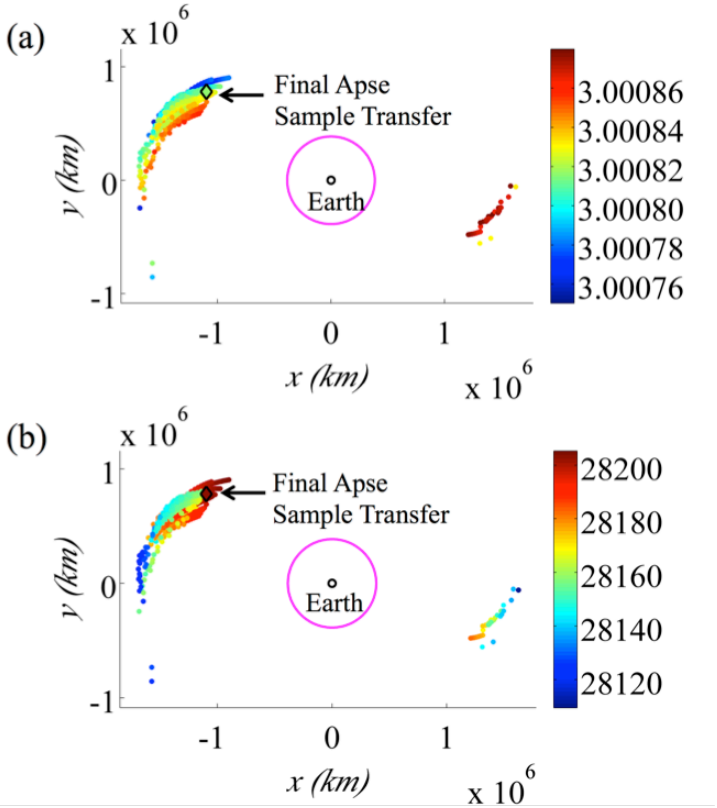


**Figure 16. Comparison of sample transfer to science orbit capture states in configuration space in the Sun-Earth rotating frame, colored by (a) Jacobi constant and (b) epoch in modified Julian date.**

possess two nearby apses that occur at similar epochs. To identify these connections, apses with similar planar projections, epochs, and energies can be located by overlaying apse maps from the Sun-Earth-Moon transfer segment with apse maps from the lunar approach segment. To verify this process, planar projections of the locations of retrograde apogees in the Sun-Earth rotating frame that result in lunar approach arcs are displayed in Figure 16. Overlaid on this plot are the location of the Earth indicated by a circle, and a circular approximation for the lunar orbit in magenta. Each colored apogee in this figure reaches a valid science orbit, one that possesses an acceptable value of RAAN, and bridges to these orbits at various values of epoch and TA. The final retrograde apoapsis from the sample trajectory is overlaid on the map as a large diamond. Each point in this map is colored by Jacobi constant in Figure 16(a) and by epoch (in modified Julian date form) in Figure 16(b). A nearby lunar approach apse that matches the color of the sample transfer apse in both maps is sought, indicating similar energy and epoch, and potentially providing a good initial guess for an end-to-end transfer. Recall that these maps represent a planar

projection of the position of the apogees, resulting in potential discontinuities in a direction normal to the ecliptic plane. Nevertheless, apses that are close in epoch, Jacobi constant and the planar position variables may still rapidly yield a good initial guess that may be otherwise challenging to identify. As an example of locating potential connections, a lunar approach apogee is located near the sample transfer apse. This apogee is then propagated forwards in time using the low-thrust enabled ephemeris model available in GMAT. The resulting lunar approach arc is plotted in the Sun-Earth rotating frame in orange, along with the sample Sun-Earth-Moon transfer in blue in Figure 17(a). Although the initial guess possesses a visible discontinuity, a corrections algorithm can be applied to reduce this discontinuity by varying the parameters along the transfer including thrust direction, burn duration, epoch, lunar flyby conditions and final science orbit parameters within the acceptable range. Furthermore, a low-thrust arc may be used to eliminate this discontinuity. As an example, this initial guess is used to produce a continuous trajectory that has been exported to GMAT, as displayed in Figure 17(b). This trajectory begins at the first apogee and leverages both natural (green) and low-thrust enabled (red) arcs to ensure lunar capture. Once the deployment conditions are known, a low-thrust arc and lunar flyby can be used to target this first apogee and, therefore, a trajectory that can deliver the spacecraft to the final science orbit.

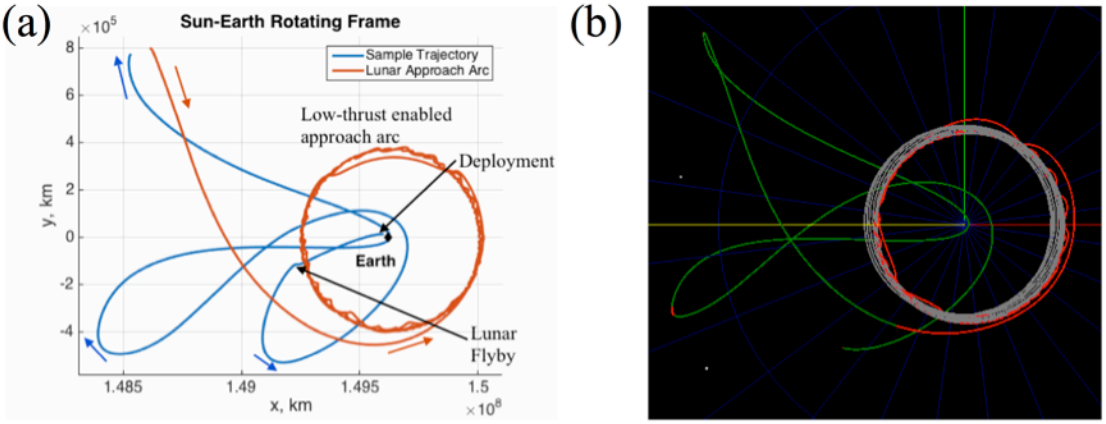


**Figure 17. (a) An initial guess constructed using a Sun-Earth-Moon segment (blue) and a lunar approach arc (orange). (b) Sample corrected trajectory in GMAT incorporating natural (green) and low-thrust (red) arcs, beginning at the first apogee. Both trajectories are displayed in the Sun-Earth rotating frame.**

## CONCLUDING REMARKS

To facilitate trajectory design for the Lunar IceCube mission, which is subject to constraints and uncertainties in its deployment state and a limited propulsive capability, a framework is constructed using techniques from dynamical systems theory. Although feasible point solutions can be identified using operational-level modeling software, a dynamical systems approach supplies insight into the sensitivity of these paths and regions of availability for similar transfers. Such analysis is valuable for spacecraft that are unable to implement large corrective maneuvers to remain on a precomputed path. To achieve a transfer between a constrained deployment state and the desired lunar science orbit, a flexible design process is constructed that enables rapid trajectory re-design to mitigate state uncertainties, orbit determination errors, and maneuver execution errors. This framework separates the Lunar IceCube trajectory into three segments for analysis: the post-deployment lunar encounter, Sun-Earth-Moon transfer, and lunar approach. Each mission segment is analyzed individually by leveraging dynamical systems techniques, applied to models of varying levels of fidelity, including the Circular Restricted Three-Body Problem and the Bi-Circular Restricted Four-Body Problem. These structures offer useful insights into the motion observed in

ephemeris propagations, and may supply preliminary bounds on transfers exhibiting a desired geometry. Poincaré maps are constructed to represent data from each mission segment. These maps are overlaid and compared to identify potential connections between transfer arcs. Once a set of feasible connections has been identified, a corrections scheme may be applied to produce an end-to-end trajectory in operational-level software. Identification of feasible transfer regions can facilitate the overall design process by providing viable solutions for contingency planning and optimization.

## ACKNOWLEDGMENTS

This work was completed at NASA Goddard Space Flight Center and at Purdue University under NASA Grant NNX13AM17G. The authors wish to thank Purdue University's School of Aeronautics and Astronautics and College of Engineering for their support, as well as the Zonta International Amelia Earhart Fellowship.

## REFERENCES

1. G. Norris, "Secondary Payloads Overview", Accessed January 2016 at: https://www.nasa.gov/sites/default/files/files/Secondary-Payloads-Overview-Rev2.pdf
2. Spacedaily.com, "Space Launch System to Boost Science with Secondary Payloads" Accessed January 2016 at: http://www.spacedaily.com/reports/Space_Launch_System_to_Boost_Science_with_Secondary_Payloads_999.html.
3. D. Folta, M. Woodard, K.C. Howell, C. Patterson, W. Schlei, "Applications of Multi-Body Dynamical Environments: The ARTEMIS Transfer Trajectory Design," *Acta Astronautica*, Vol. 74, 2012, pp. 237-249.
4. P.E. Clark, B. Malphrus, R. MacDowall, D. Folta, A. Mandell, C. Brambora, D. Patel, S. Banks, K. Hohman, V. Hruby, K. Brown, J. Kruth, R. Cox, "Lunar Ice Cube: Determining Volatile Systematics Via Lunar Orbiting Cubesat," *European Planetary Science Congress 2015*, Vol. 10.
5. Busek.com, "3cm RF Ion Thruster" Accessed January 2016: http://www.busek.com/index_htm_files/70010819%20RevA%20Data%20Sheet%20for%20BIT-3%20Ion%20Thruster.pdf.
6. A. Haapala, M. Vaquero, T. Pavlak, K.C. Howell, D. Folta, "Trajectory Selection Strategy for Tours in the Earth-Moon System," AAS/AIAA Astrodynamics Specialist Conference, Hilton Head, South Carolina, August 2013.
7. General Mission Analysis Tool. Available: gmatcentral.org. Software package, 2016.
8. Systems Tool Kit, Software Package, Analytical Graphics Inc., 2016.
9. V. Szebehely, *Theory of Orbits: The Restricted Problem of Three Bodies*. London, UK: Academic Press, 1967.
10. W.S. Koon, M.W. Lo, J.E. Marsden, and S.D. Ross, *Dynamical Systems, The Three Body Problem and Space Mission Design.* Springer-Verlag, New York Incorporated, 2011.
11. G. Gómez, W.S. Koon, M.W. Lo, J.E. Marsden, S.D. Ross, J.J. Masdemont, "Invariant Manifolds, the Spatial Three-Body Problem and Petit Grand Tour of Jovian Moons," Libration Point Orbits and Applications, Aiguablava, Spain, June 2002.
12. T.S. Parker, L.O. Chua, *Practical Numerical Algorithms for Chaotic Systems*, New York: Springer-Verlag, 1989.
13. A.E. Roy, B.A. Steves, *From Newton to Chaos: Modern Techniques for Understanding and Coping with Chaos in N-Body Dynamical Systems*, Vol. 336 of Nato Science Series B, Chapter 4.
14. A. Cox, K.C. Howell, "Transfers to a Sun-Earth Saddle Point: An Extended Mission Design Option for LISA Pathfinder," AAS/AIAA Space Flight Mechanics Meeting, Napa, California, February 2016.